Confined nanorods: Jamming due to helical buckling

Daniel Svenšek[1] and Rudolf Podgornik[1,2]

[1]*Department of Physics, Faculty of Mathematics and Physics, University of Ljubljana, Jadranska 19, SI-1111 Ljubljana, Slovenia*
[2]*Department of Theoretical Physics, J. Stefan Institute, Jamova 39, SI-1000 Ljubljana, Slovenia*

We investigate a longitudinally loaded elastic nanorod inside a cylindrical channel and show within the context of classical elasticity theory that the Euler buckling instability leads to a helical postbuckling form of the rod within the channel. The local pitch of the confined helix changes along the channel and so does the longitudinal force transmitted along the rod, diminishing away from the loaded end. This creates a possibility of jamming of the nanorod within the channel.

PACS number(s): 36.20.−r, 62.25.−g, 61.46.Fg, 62.20.mq

I. INTRODUCTION

Elastic instabilities of nanoscale rods and in particular the Euler (buckling) instability have long been recognized as being essential for structural as well as functional aspects of nano- and biosystems. Some time ago [1] Manning proposed that DNA collapse in polyvalent salt solutions proceeds through a type of Euler buckling driven by diminished electrostatic repulsive interactions between charged phosphates along the DNA backbone. Though the details of his picture appear to be speculative, the general framework has been completely vindicated by later work [2]. Buckling instability also appears to play an important part in the conformation of linker DNA within the chromatin fiber [4], in the case of a growing microtubule pushing against a microfabricated rigid barrier [3], and in the stability of atomic force microscope (AFM) tips, nanotubes [5], and nanorods [6].

The confinement of nanoscale rods to micro- and nanochannels presents yet another set of experimental and theoretical problems [7] centered around the technological challenges of manufacturing nanopores and nanochannels for investigating and manipulating DNA. Here the main theoretical thrust is in the direction of understanding the various contributions to the confinement free energy that depend on the size of the confining space and the intrinsic properties of the confined nanorods. The behavior of confined semiflexible polymers is particularly important in this context and has been recently analyzed in detail [8,9]. In many respects this type of problem is mainly centered upon transverse confinement, whereas the elastic instabilities described before are due to longitudinal confinement of elastic rods.

Motivated by these phenomena, we will try in what follows to combine the two aspects of polymer confinement described above, considering an elastic buckling instability within a confining cylindrical channel. The confinement of the elastic rod is thus twofold: longitudinal, leading to buckling, and transverse, leading straightforwardly to a helical postbuckling form. We will show that transverse confinement with frictional walls furthermore leads to a decay of the longitudinal force within the rod along the long axis of the confining channel. This will not be too difficult to rationalize, since we know from other systems that longitudinal stresses can be taken up effectively by friction at confining walls. For a silo filled with granular matter and compressed on one side by a force F_0, Janssen's equation [10] gives an exponential decrease of the compression force with increasing distance z from the compressed side,

$$F(z) = F_0 \exp(- \lambda k_{\mathrm{fr}} z \mathcal{P}/\mathcal{S}),$$

where $\lambda = \sigma_{rr}/\sigma_{zz}$ is the ratio of horizontal and vertical stresses, $\mathcal{P}/\mathcal{S}$ is the ratio of the perimeter to the cross-section area, k_{fr} is the static friction coefficient, and we have neglected gravity. The same holds also for a regular elastic solid, i.e., a rigidly confined rod, if one neglects lateral deformation gradients in the rod [11]. There we have

$$F(z) = F_0 \exp[- \sigma k_{\mathrm{fr}} z \mathcal{P}/\mathcal{S}(1 - \sigma)],$$

where σ is Poisson's ratio. On this simple basis one expects also a conceptually similar effect, i.e., a decrease of compression force with increasing distance along an elastic rod confined to a cylindrical channel in the postbuckling regime. This will allow us to hypothesize about the existence of a jamming regime for sufficiently long confined elastic rods.

The plan of this paper is as follows. We shall first present the classical elastic model for an Eulerian rod and derive the scaling relations valid for the onset of the buckling instability. We shall solve an approximate form of the elastic equations within a cylindrically confined channel and show that the longitudinal force, at least within the considered approximations, decays in inverse proportion to the length of the confining channel when friction at the cylindrical wall is taken into account. To obtain exact solutions of the elastic equations we will proceed numerically and derive the minimal shape of the confined rod and the magnitude of the transmitted longitudinal force along the axis of the confining channel. At the end we will discuss the possible conditions that would lead to a jamming of the elastic rod within the cylindrical confining channel.

II. ELASTIC MODEL

We model the rod as a thin Eulerian elastic filament to which the standard continuum theory of elasticity can be applied. The confining channel is modeled as a straight cylindrical tube with rigid walls. The ratio R/L of tube radius R and undeformed filament length L is the relevant geometric parameter of the system.

Let us briefly review the equilibrium equations for thin elastic rods [12]. The force balance reads

$$\frac{d\mathbf{F}}{dl} + \mathbf{K} = \mathbf{0}, \tag{1}$$

where dl is the length element on the rod (l is the natural parameter—the length along the filament), $\mathbf{F}$ is the elastic force exerted on the leading surface of the rod element [in the sense of increasing l; the force on the opposite (trailing) side is $-\mathbf{F}$, of course], and $\mathbf{K}$ is the external force per unit length. The torque balance reads

$$\frac{d\mathbf{M}}{dl} + \mathbf{t} \times \mathbf{F} = \mathbf{0}, \tag{2}$$

where $\mathbf{M}$ is the elastic torque exerted about the center of the leading surface and $\mathbf{t}$ is the unit tangent of the rod. The elastic torque is related to the deformation of the filament via

$$\mathbf{M} = G\tau\mathbf{t} + EI\mathbf{t} \times \dot{\mathbf{t}}, \tag{3}$$

where E is the Young modulus and we assumed that the rod is circular, i.e., both geometric moments of inertia of the cross section are equal, $I = \int dS\, x^2 = \int dS\, y^2$. The first term on the right of Eq. (3) describes torsion, which we assume to be absent. One can show that in the case of an isotropic moment of inertia, torsion is absent everywhere in the rod when there is no twisting torque applied [12]. In what follows, the twisting (torsional) torque will be absent, i.e., the torque in the rod will have a vanishing tangential component,

$$\mathbf{M} = EI\mathbf{t} \times \dot{\mathbf{t}}. \tag{4}$$

From Eqs. (2) and (4) one then gets

$$EI\mathbf{t} \times \ddot{\mathbf{t}} + \mathbf{t} \times \mathbf{F} = \mathbf{0} \tag{5}$$

as the fundamental equation describing the shape of the bent filament. The solutions of this equation with various boundary conditions are discussed in standard references on the theory of elasticity [12].

A. Buckling in confined geometry

It is well known that, when a straight rod is compressed by an axial force, above threshold it undergoes a buckling instability—the so-called Euler buckling—and becomes bent. For a rod with hinged ends or ends that are laterally free (both situations are identical in this case), for example, the threshold force is $F_{\text{crit}} = EI\pi^2/L^2$ [12].

What happens when the (thin) rod is confined within a rigid cylinder? Once the compressing force is sufficiently large that the bent rod touches the wall of the cylinder (let it be bent in the diameter plane) and is further increased, there are two scenarios one can think of: the rod can bend back and forth, staying in the diameter plane, or it can become a helix touching the cylinder wall (springlike configuration). In the oil-drilling community it has been recognized for a long time that it is the latter that eventually happens [13–16] (In fact, this is the only area of research where helical buckling has been studied.) It turns out, as we will show in Sec. V, that there indeed exists a secondary threshold above which the planar configuration is unstable with respect to the helix.

B. Scaling

By the introduction of dimensionless quantities denoted with a tilde,

$$l = R\tilde{l}, \quad \mathbf{F} = \frac{EI}{R^2}\tilde{\mathbf{F}}, \quad \mathbf{K} = \frac{EI}{R^3}\tilde{\mathbf{K}}, \quad \mathbf{M} = \frac{EI}{R}\tilde{\mathbf{M}}, \tag{6}$$

Eqs. (1)–(5) attain a universal form. Thus, the solutions depend only on the aspect ratio L/R. If the system size is rescaled and the aspect ratio is preserved, the solution is unchanged if the forces and torques of the boundary condition are also rescaled correspondingly, i.e., according to Eq. (6). Similarly, taking a rod with a different EI and rescaling the forces and torques does not affect the solution.

III. ANALYTIC DESCRIPTION OF THE HELIX

A. Simple model

Let us write down equilibrium equations for a helically deformed filament constrained to and lying on a cylindrical surface of radius R. The deformation is sustained by an external compressing force $F_z < 0$ parallel to the long axis of the cylinder. We disregard the transition regions in the vicinity of both ends and focus on the central part of the long helix, i.e., we assume that its pitch is constant. Friction is absent at this stage.

In cylindrical coordinates (r, ϕ, z) the helix is given by $r = R$ and the linear function $\phi(l)$. The tangent is thus given by

$$\mathbf{t} = \frac{d\mathbf{r}}{dl} = R\dot{\phi}\hat{\mathbf{e}}_\phi + \sqrt{1 - (R\dot{\phi})^2}\hat{\mathbf{e}}_z. \tag{7}$$

Further, we put $\mathbf{F} = F_r\hat{\mathbf{e}}_r + F_\phi\hat{\mathbf{e}}_\phi + F_z\hat{\mathbf{e}}_z$, where the first two components are unknown and must be determined. The force of the cylinder per unit length is $\mathbf{K} = -K\hat{\mathbf{e}}_r$. Equation (5) then reads

$$[\sqrt{1 - (R\dot{\phi})^2}(EIR\dot{\phi}^3 - F_\phi) + R\dot{\phi}F_z]\hat{\mathbf{e}}_r + \sqrt{1 - (R\dot{\phi})^2}F_r\hat{\mathbf{e}}_\phi$$
$$- R\dot{\phi}F_r\hat{\mathbf{e}}_z = \mathbf{0}. \tag{8}$$

Equation (8) requires

$$F_r = 0, \tag{9}$$

while from Eq. (1) one gets

$$F_\phi = -\frac{K}{\dot{\phi}} \tag{10}$$

and hence for the radial component of Eq. (8)

$$\sqrt{1 - (R\dot{\phi})^2}(EIR\dot{\phi}^4 + K) + R\dot{\phi}^2 F_z = 0. \tag{11}$$

Now comes a crucial point. The equilibrium condition (11) involves both the helical deformation $\dot{\phi}$ and the external force $\mathbf{K}$, so additional input is needed to determine one or the other. This comes from the boundary condition, which is, however, inaccessible under the assumption of fixed pitch.

Let us digress a little and illustrate in physical terms why the force of the cylinder, $\mathbf{K}$, cannot be specified until the

boundary condition is known. In addition to the force $\mathbf{F}$, the boundary condition involves also the torque exerted on the free ends (which must be normal to the tangent of the rod as we are not considering torsion). By using a pair of wrenches and applying torque to the ends, one changes the force exerted on the cylinder wall. Using just the right torque, for example, one can make $\mathbf{K}$ vanish. When the torque is increased further, the rod detaches from the cylinder and forms a free helix with the radius smaller than R [17]. According to Eqs. (4) and (7), the torque in the filament is

$$\mathbf{M} = EIR\dot{\phi}^2[-\sqrt{1-(R\dot{\phi})^2}\hat{\mathbf{e}}_\phi + R\dot{\phi}\hat{\mathbf{e}}_z]. \qquad (12)$$

In fact, with this torque applied to the ends (together with F_ϕ and F_z), the helical pitch is constant everywhere. By changing the torque, one changes the pitch, Eq. (12), and therewith the cylinder force $\mathbf{K}$, Eq. (11). Note that there is no tangential force in the free (detached from the cylinder) helix, Eq. (10).

When there is no torque applied to the ends, i.e., when the rod is compressed inside the cylinder by a pair of pistons, the part of the rod close to the end detaches from the wall while the tip (which is straight due to zero torque) pushes against the wall with a discrete force (see the numerical solutions in Fig. 1). The torque due to this force increases as we move away from the tip and eventually becomes sufficiently large for the helical deformation.

Let us return to the case of a constant helical pitch. One can invoke an energy argument to independently estimate the dependence of $\dot{\phi}$ on the compressing force F_z. The elastic free energy of the compressed helix without the contribution of the torsion is

$$\mathcal{F} = \frac{1}{2}EI\int_0^L dl|\dot{\mathbf{t}}|^2 - L_z F_z, \qquad (13)$$

where L is the length of the filament and L_z is the length of its projection on the z axis, i.e., the length of the coil. Recall that $F_z < 0$. With Eq. (7) and $dz/dl = \sqrt{1-(R\dot{\phi})^2} = L_z/L$, we have

$$\mathcal{F} = \frac{1}{2}EIL(R\dot{\phi}^2)^2 + L\sqrt{1-(R\dot{\phi})^2}|F_z|, \qquad (14)$$

and after minimizing, in the lowest order of $R\dot{\phi}$,

$$\dot{\phi}^2 = \frac{|F_z|}{2EI}. \qquad (15)$$

Hence, from Eq. (11) one gets a direct relation between the load and the wall forces. To the lowest order the force of the cylinder is

$$K = \frac{R}{2EI}F_z^2. \qquad (16)$$

So far friction has been absent. Let us now consider it as a perturbation and introduce a small friction coefficient k_{fr}. One is aware, of course, that for finite friction the constant pitch is not a solution, neither can one use the energy argument. We are interested in how the compressing force $|F_z|$ is
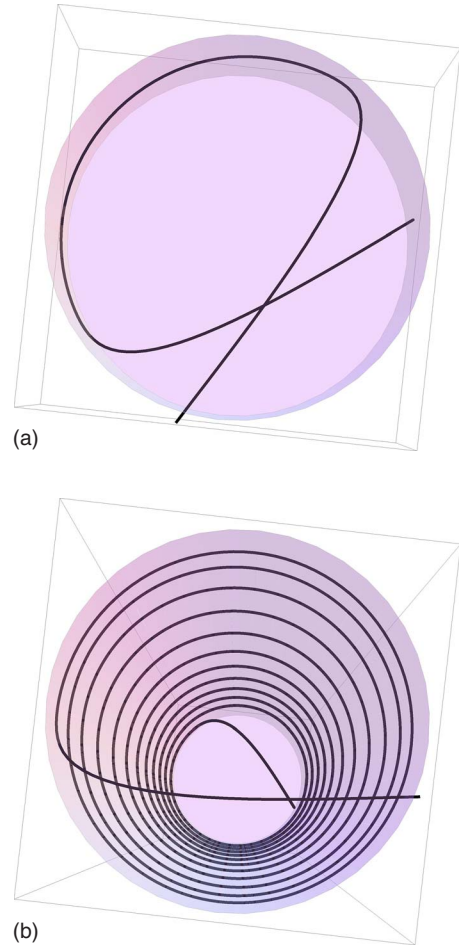

(a)

(b)

FIG. 1. (Color online) A long-axis view of helical filaments with lengths $L/R=$ (a) 20 and (b) 640, buckled by a force $|F_z(0)| = 0.25EI/R^2$, which is approximately (a) 10 and (b) 10 000 times the critical force for Euler buckling, $F_{crit}=EI\pi^2/L^2$. There is no torque applied to the ends.

reduced by the friction in going from one end of the helix to the other. Let us assume that the helix is compressed by the external force F_{z0} at $l=0$ and that the friction is parallel to z, opposing the external force. Assuming the static friction is maximum everywhere, it follows from the force balance (1) that

$$\frac{d|F_z|}{dl} = -k_{\text{fr}}K. \qquad (17)$$

Combining Eqs. (16) and (18), we finally get

$$|F_z(l)| = \left(\frac{1}{|F_{z0}|} + \frac{k_{fr}R}{2EI}l\right)^{-1}. \qquad (18)$$

The virtual point where F_z would diverge lies at

$$l_c = -2EI/k_{\text{fr}}R|F_{z0}|, \qquad (19)$$

which thus dictates the extent of the reduction of the compression force. The smaller is $|l_c|$, the stronger is the decay of the force. Increasing k_{fr}, $|F_{z0}|$, or R reduces $|l_c|$ and moves the singular point closer to the beginning of the helix. Equation

(18) can be put into a universal form by introducing the force unit $F_0 = 2EI/k_{fr}RL$,

$$\frac{|F_z(l)|}{F_0} = \left(\frac{F_0}{|F_{z0}|} + \frac{l}{L}\right)^{-1}. \tag{20}$$

Note in Eq. (6) that, if the aspect ratio is constant, the force scales as $1/R^2$ (or equivalently $1/L^2$). This, of course, always holds and is approximation independent. In addition, the result (20) of our simple model gives a $1/RL$ scaling of the force when the aspect ratio is changed; this, however, is only an approximation.

B. Exact analysis

For completeness, let us derive exact equilibrium equations for the helically buckled filament in the presence of friction. We do not aim to solve them, yet they will be helpful giving us insight into the solution. As before, the filament is assumed to lie on the cylinder everywhere, $r = R$, but now all variables are l dependent, including the compressing force F_z.

Equation (5) involves only two components as it is orthogonal to **t**. Therefore we project it to $\hat{\mathbf{e}}_r$ and the direction $\mathbf{t} \times \hat{\mathbf{e}}_r$. Writing $\dot{\phi}(l) = \omega(l)$, the former is

$$\frac{EIR}{(1 - R^2\omega^2)^{3/2}}[\omega^3(1 - R^2\omega^2)^2 - \ddot{\omega}(1 - R^2\omega^2) - R^2\omega\dot{\omega}^2]$$
$$- F_\phi\sqrt{1 - R^2\omega^2} + F_z R\omega = 0 \tag{21}$$

and the latter

$$-\frac{3}{2}EIR\frac{d}{dl}(\omega^2) + F_r = 0. \tag{22}$$

Again we choose from an infinite number of solutions, which exist when the static friction is involved, the simplest and most symmetric one, in which the friction is everywhere at its maximum and parallel to z. With $\mathbf{K} = K(l)(-\hat{\mathbf{e}}_r + k_{fr}\hat{\mathbf{e}}_z)$ the three components of the force balance (1) are

$$(\dot{F}_r - \omega F_\phi - K)\hat{\mathbf{e}}_r = \mathbf{0}, \tag{23}$$

$$(\omega F_r + \dot{F}_\phi)\hat{\mathbf{e}}_\phi = \mathbf{0}, \tag{24}$$

$$(\dot{F}_z + k_{fr}K)\hat{\mathbf{e}}_z = \mathbf{0}. \tag{25}$$

Equations (21)–(25) represent a closed set of five ordinary differential equations for the five variables $\omega(l)$, $K(l)$, and $\mathbf{F}(l)$. One can verify that, in the case $\dot{\omega} = 0$, Eqs. (9)–(11) are recovered.

One can expand the system (21)–(25) for small $R\omega$. For $k_{fr} \neq 0$, terms of third order must be included to get a solution [one can check that the second order gives only the second-order part of the stationary solution (9)–(11) for $k_{fr} = 0$, and no solution for $k_{fr} \neq 0$]. Inserting Eq. (22) into Eq. (24) and integrating, one gets a partial result $F_\phi = A - EI\omega^3$, where A is a constant.

IV. NUMERICAL APPROACH

We will solve the fundamental equations for the actual deformation of the compressed and confined filament numerically for it is only in this way that one can obtain a complete solution of the problem. The filament is naturally allowed to detach from the wall, which essentially takes place near the two ends of the filament, and the helix within the cylindrical pore can form spontaneously without having been put in "by hand." Let us stress again that the solution, including in particular the pitch of the bulk helix and the force exerted on the cylinder wall, is determined only when the ends of the filament are taken into account, which furthermore inevitably involves detachment of the filament from the wall unless the boundary condition is very special, as explained in Sec. III A, Eq. (12).

For the purpose of numerical modeling that involves discretization, it is generally better, if possible, to start with a discrete analog of the continuum system and write down algebraic equations, rather than discretizing the differential equations themselves, derived for the continuum limit. In this spirit, the elastic filament will be represented as a set of straight and stiff elements (links) of fixed length l_0 with forces and torques acting between them. The element i is described by its center of mass $\mathbf{r}_i$ and a unit (tangent) vector $\mathbf{t}_i$ giving its orientation. Dynamical evolution of the filament shape is obtained by Newton's laws for translation and rotation of each element.

The joints between the links are rather cumbersome to model: they act as constraints for the ends of the two elements, which must meet in a single point, and thus exert constraint forces that can be determined only implicitly, such that the elements satisfy the constraints. To avoid this, we relax (soften) the constraints and introduce a quadratic (bond) penalty potential

$$V(\mathbf{r}_i^+, \mathbf{r}_{i+1}^-) = \frac{k}{2}|\mathbf{r}_{i+1}^- - \mathbf{r}_i^+|^2, \tag{26}$$

where $\mathbf{r}_i^+ = \mathbf{r}_i + (l_0/2)\mathbf{t}_i$ and $\mathbf{r}_{i+1}^- = \mathbf{r}_{i+1} - (l_0/2)\mathbf{t}_{i+1}$ are the two ends meeting at the joint. The coefficient k should be sufficiently large so that the gap between the ends is small compared to the element length, $|\mathbf{r}_{i+1}^- - \mathbf{r}_i^+| \ll l_0$. The sidewall of the cylinder is modeled in a similar manner, introducing a wall penalty potential

$$V_w(\mathbf{r}_i^\pm) = \begin{cases} \dfrac{k_w}{2}(|\mathbf{r}_i^\pm| - R)^2, & |\mathbf{r}_i^\pm| > R, \\ 0, & |\mathbf{r}_i^\pm| \leq R. \end{cases} \tag{27}$$

Again the coefficient k_w should be sufficiently large so that $|\mathbf{r}_i^\pm| - R \ll l_0$. The forces on the ends of the elements are

$$\mathbf{F}_i^\pm = -\frac{\partial V}{\partial \mathbf{r}_i^\pm} - \frac{\partial V_w}{\partial \mathbf{r}_i^\pm}. \tag{28}$$

It makes little difference (i.e., no difference in the limit $l_0 \to 0$) whether the force of the wall actually acts on both ends or just at the center of the element.

Torques about the center of element i are of two kinds. One comes from elastic couples exerted by the two neigh-
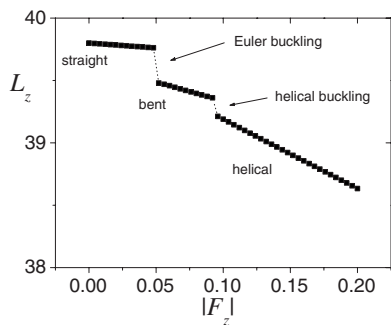
FIG. 2. External load dependence of the projection of filament length onto the axis of the confining cylindrical pore. The weak force dependence of length in the straight configuration is due to the small artificial compressibility introduced by the penalty potential (26) (i.e., finite value of the spring constant k). In the limit of zero compressibility this part of the functional dependence would be a straight horizontal line.

boring elements and the other from the forces on both ends of element i:

$$\mathbf{M}_i = C\mathbf{t}_i \times (\mathbf{t}_{i-1} + \mathbf{t}_{i+1}) + \frac{l_0}{2}(\mathbf{t}_i \times \mathbf{F}_i^+ - \mathbf{t}_i \times \mathbf{F}_i^-), \quad (29)$$

where C is the bending stiffness, which we shall connect to continuum parameters. In the continuum picture, the first part of the torque translates to the first term of Eq. (5) and the second part to the second term of Eq. (5).

To get the evolution of the shape of the filament, we conveniently assume overdamped dynamics:

$$\beta \frac{d\mathbf{r}_i}{dt} = \mathbf{F}_i^+ + \mathbf{F}_i^-, \quad (30)$$

$$\beta \frac{d\mathbf{t}_i}{dt} = \beta \frac{d\varphi_i}{dt} \times \mathbf{t}_i = \mathbf{M}_i \times \mathbf{t}_i, \quad (31)$$

where β is an arbitrary damping coefficient defining the time scale.

One can verify that the set of discrete equations (29)–(31) agrees with properly discretized continuum equations with the following connection between the parameters:

$$C = \frac{EI}{l_0^2}, \quad (32)$$

while $\beta = l_0 \beta_{ph}$, where β_{ph} is the physical (continuum) damping coefficient. The latter is only important for properly scaling the time when the element length l_0 is changed in the numerical model. Similarly, $k = k_{ph}/l_0$ to ensure that the spring constant k_{ph} of the rod [which is infinite in the continuum description (1)–(4) of a thin rod] is unaffected by changes of l_0.
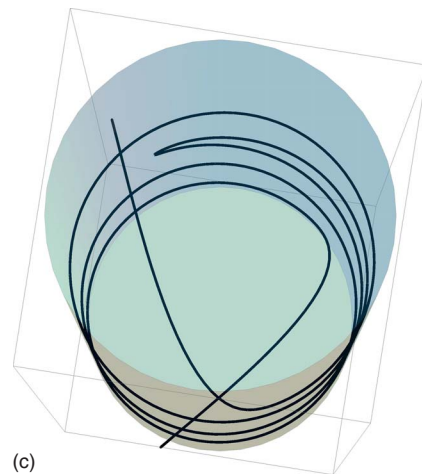
To avoid giant friction forces in certain discrete points (e.g., a few points around the detachment region which exert a large force on the confining wall), the friction force is properly capped, so that the Coulomb friction law is violated in these few points but met everywhere else.
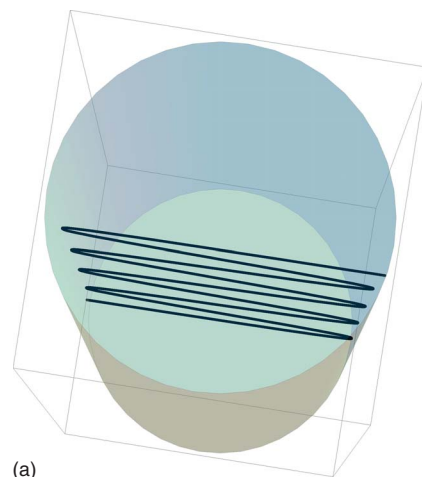
(a)
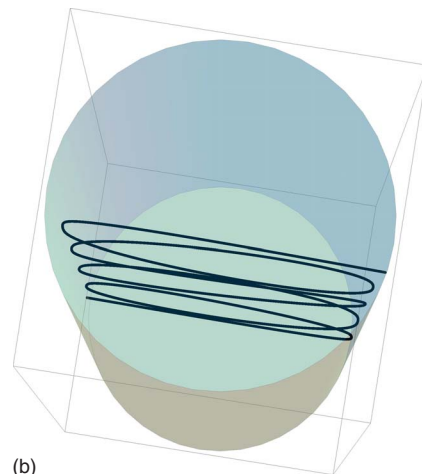
(b)

(c)

FIG. 3. (Color online) Planar configuration of the confined filament (a) is unstable (b) and is transformed into the helical configuration (c) upon perturbation. The helix can contain metastable irregularities as seen in the equilibrium state (c).

V. RESULTS

First let us take a look at numerical solutions of helically buckled filaments. Figure 1 shows two examples of filaments of different lengths buckled by the same axial force. We use
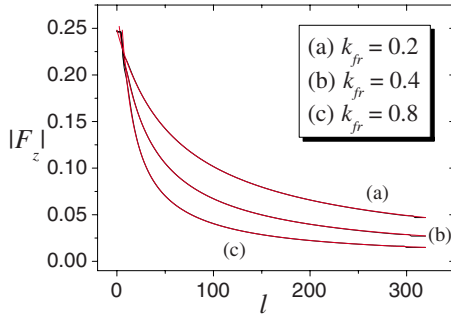
FIG. 4. (Color online) Compression force profile $|F_z(l)|$ in a filament with length to radius ratio 320. The loading force is $|F_z(0)|=0.25EI/R^2$, which is approximately 2600 times the critical force for Euler buckling, $F_{crit}=EI\pi^2/L^2$. Numerical data (black) are excellently fitted (red) with the function $f(l)=A(l_0+l)^c$ (the curves are perfectly overlapping on the scale of the figure): (a) $A=36.3$, $l_0=285.5$, $c=-0.882$; (b) $A=21.4$, $l_0=131.8$, $c=-0.894$; (c) $A=11.95$, $l_0=44.9$, $c=-0.903$.

the most natural boundary condition: the upper (compressed) end is merely pushed along z (the cylinder axis), while the lower end is not allowed to move in the z direction. Both ends are free to move laterally until they hit the confining wall. There is no torque applied to them. To build up the torque exerted on the filament cross section in the helical state, however, the ends must leave the helical state as anticipated in Sec. III A.

To numerically study the solution path from the straight to the helical configuration, we introduce a tiny random perturbation to the straight compressed filament. A numerically obtained state diagram is depicted in Fig. 2, where a suitable parameter distinguishing between the configurations is simply the projection of the filament length onto the z axis. There exist two threshold forces beyond which the straight and the Euler-buckled states are unstable, respectively. The helical state is a consequence of the confinement and sets in after the filament has touched the wall. Above the threshold, the planar state remains a solution but is unstable with respect to the helix, which is demonstrated in Fig. 3. There one also sees a defect in the helix. Such defects are a general feature subject to the initial condition (perturbation) and are metastable, i.e., they are stable while the compressing force is not reduced.

We are furthermore interested in the force that has to be applied to the lower end to keep it fixed, i.e., to sustain the confined helix. As we are to show, this force can be much less than the load applied to the upper end due to the action of friction and in fact approaches zero for very long confining channels. This opens up the possibility of jamming, i.e., of a stable static helical configuration of the rod that has been jammed against the confining walls via the surface friction and is sustained with only a tiny (zero in the limit of a very long channel) opposing force at the other end of the channel.

Figure 4 shows the profiles of the longitudinal force $|F_z|$ as we move along the filament, and Fig. 5 shows the profile of the helical deformation $\dot\phi$. The force profiles are perfectly fitted by a power law, yet with an exponent close to -0.9 instead of -1 as suggested by Eq. (18). The validity of the power law is remarkable, though it deviates from the ap-
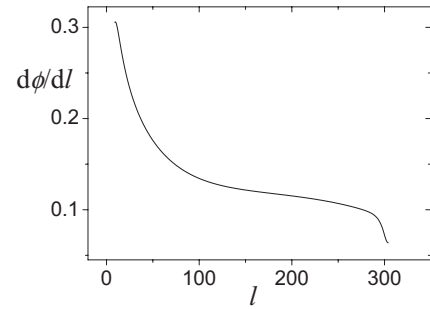

FIG. 5. Profile of $d\phi/dl$, the inverse of the helical pitch $q_0=2\pi/(d\phi/dl)$, for the filament of Fig. 4(c). The boundaries where the pitch is not defined are not displayed. As expected, $\dot\phi$ gets smaller (the pitch gets larger) as the longitudinal force is reduced. Its relative decrease is, however, smaller than that of the force, as hinted by the quadratic dependence $F_z \propto \dot\phi^2$ in Eq. (15) of the simple model (which assumes constant pitch).

proximate universal scaling of Eq. (20). In other words, the solution is practically indistinguishable from a power law, in spite of the evidence that it considerably departs from our simple model. The reason for this remarkable validity of the power law, yet with an exponent different from -1, is not clear. Figure 6 shows the force transmitted to the lower end as a function of the length L of the filament, at a fixed load on the upper end. We see that for long filaments the transmitted force is strongly reduced and asymptotically approaches zero.

The physically interesting interval of loading force strengths depends on the aspect ratio of the filament. In Fig. 4, for example, the loading force was selected such that the transmitted force was significantly reduced. The reduction of the transmitted force is weaker if the loading force is smaller, Fig. 7, in accord with Eq. (19) of the simple model. On the other hand, increasing the loading force beyond a threshold (that scales as $1/R^2$) results in a catastrophic event—a U bending of the filament, leading to escape out of the confining pore, Fig. 8. Hence, it is only for long and thin rods that the transmitted force can be strongly reduced.

VI. DISCUSSION

In this work we have analyzed the behavior of an elastic filament that is confined in the longitudinal as well as the
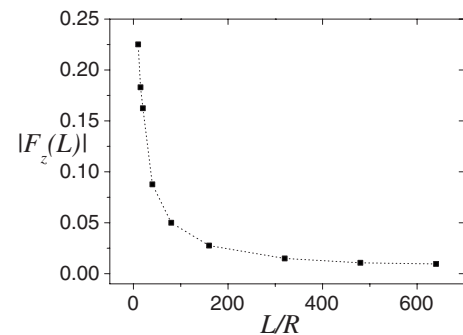

FIG. 6. Compression force $|F_z(L)|$ transmitted through filaments of length L; the external compressing force is $|F_z(0)|=0.25EI/R^2$; $k_{fr}=0.8$. The dotted line serves as a guide to the eye.
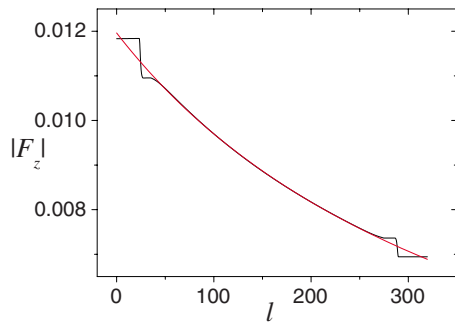
FIG. 7. (Color online) Compression force profile $|F_z(l)|$ (black) in the filament with length to radius ratio 320 for a smaller loading force $|F_z(0)|=0.0125EI/R^2$ and $k_{\mathrm{fr}}=0.8$, fitted (red) with the function $f(l)=A(l_0+l)^c$; $A=15.5$, $l_0=2010$, $c=-0.942$. The reduction of the force is much smaller than for larger loads in Fig. 4, on account of the singular point l_c in Eq. (19) moving further away. The exponent of the power law, however, remains nearly unchanged. The boundary regions get wider as the load is reduced.

transverse direction. The longitudinal confinement leads to the well-known Euler buckling instability which depends on the external loading and the length of the filament. We have shown that the buckled configuration, on touching the confining walls of a cylindrical channel, then evolves through a planar deformed configuration toward a helical state via an additional instability. By considering the effects of the friction on the walls of the cylindrical enclosure, we have been able to demonstrate that the longitudinal force transmitted through the filament decays along its length. This phenomenon is not unrelated to the decaying longitudinal stresses within a cylindrical granular column anchored by the wall friction, or even a regular elastic solid with a finite Poisson ratio enclosed within a rigid hollow cylinder and again anchored by wall friction.

The important difference between the examples of granular and regular solids confined within cylindrical walls and the present case of a thin elastic filament is the nature of the decay of the longitudinal force along the cylindrical enclosure. In the first two cases the decay is exponential and leads to a natural length scale for the problem. This means that the jamming of the granular or classical elastic bodies depends only on intrinsic parameters, describing the stress distributions within the body and the magnitude of the friction forces between the body and the cylindrical enclosure. In the case of the confined filament, the longitudinal force transmitted along the cylindrical enclosure decays algebraically. In this case, the onset of jamming is determined by the intrinsic elastic parameters of the filament as well as the longitudinal force counteracting the loading from the opposite side of the enclosure. This counterforce could be in principle very small and could even result from thermodynamic fluctuations on the other end of the enclosure if the cylindrical pore is small enough. Nevertheless, the fact that the onset of jamming in the case of a confined elastic filament is scale-free and thus depends on external constraints separates it fundamentally
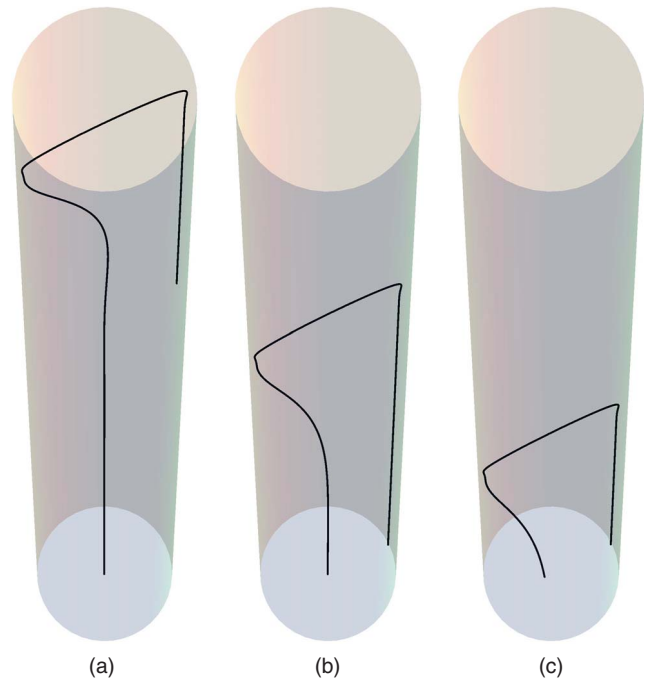

FIG. 8. (Color online) If the load is too large, the filament makes a U bend and escapes out of the cylinder, as shown on the subsequent figures instead of forming the helix. $L/R=320$, $|F_z(0)|=0.5EI/R^2$; only the upper half of the cylinder is shown.

from the standard jamming in granular materials [18].

What would be the systems that could exhibit this type of jamming scenario? We have found that the criterion for the onset of helical postinstability shape is geometrical: according to the curve in Fig. 6, the aspect ratio of polymer length (or persistence length, if it is smaller) and the radius of the pore should be of the order of 100 or more for a significant reduction of the compression force that could in principle lead to jamming. For carbon nanotubes with a typical length of 100 μm and Young's modulus of 10^{12} Pa, the relevant pore radius is 1 μm or less, and the loading force is in the nanonewton range—all reasonable values. On the other hand, DNA appears to be too flexible, i.e., its persistence length of 50 nm is too short, as it should be confined to a subnanometer pore, violating the structural integrity of DNA (the diameter of DNA is approximately 2 nm). It thus appears that at least in principle one could observe the helical instability coupled to a jamming transition within the context of confined microtubules. We hope that our theoretical work will provide enough motivation for experimentalists to search for this interesting phenomenon.

ACKNOWLEDGMENTS

[1] G. S. Manning, Cell Biophys. **7**, 57 (1985).

[2] P. L. Hansen, D. Svenšek, V. A. Parsegian, and R. Podgornik, Phys. Rev. E **60**, 1956 (1999).

[3] M. Dogterom and B. Yurke, Science **278**, 856 (1997).

[4] J-M. Victor, E. Ben-Haim, and A. Lesne, Phys. Rev. E **66**, 060901(R) (2002).

[5] B. I. Yakobson, C. J. Brabec, and J. Bernholc, Phys. Rev. Lett. **76**, 2511 (1996).

[6] E. W. Wong, P. E. Sheehan, and C. M. Lieber, Science **277**, 1971 (1997).

[7] W. Reisner, K. J. Morton, R. Riehn, Yan Mei Wang, Zhaoning Yu, M. Rosen, J. C. Sturm, S. Y. Chou, E. Frey, and R. H. Austin, Phys. Rev. Lett. **94**, 196101 (2005).

[8] F. Wagner, G. Lattanzi, and E. Frey, Phys. Rev. E **75**, 050902(R) (2007).

[9] T. Odijk, J. Chem. Phys. **125**, 204904 (2006).

[10] H. A. Janssen, Z. Ver. Dtsch. Ing. **39**, 1045 (1895).

[11] It can be shown that this is valid if the Poisson ratio σ is sufficiently small, $\sigma \ll 0.5$.

[12] L. D. Landau and E. M. Lifshitz, *Theory of Elasticity*, 3rd ed. (Reed, Oxford, 1986).

[13] A. Lubinski, W. S. Althouse, and J. L. Logan, J. Pet. Technol., 655 (1962); Trans., AIME, 225 (1962).

[14] R. F. Mitchell, SPEDE **3**, 303 (1988).

[15] R. F. Mitchell, SPE Drill. Completion **11**, 178 (1996).

[16] R. F. Mitchell, SPE J. **7**, 373 (2002).

[17] A. E. Love, *A Treatise on the Mathematical Theory of Elasticity*, 4th ed. (Dover Publications, New York, 1944).

[18] J. Duran, *Sands, Powders, and Grains: An Introduction to the Physics of Granular Materials*, 1st ed. (Springer, Berlin, 1999).